Transp Porous Med (2012) 91:81–100
DOI 10.1007/s11242-011-9834-6

Influence of Heat and Mass Transfer on Newtonian Biomagnetic Fluid of Blood Flow Through a Tapered Porous Arteries with a Stenosis

S. Nadeem · Noreen Sher Akbar · T. Hayat · Awatif A. Hendi

Received: 13 November 2009 / Accepted: 25 August 2011 / Published online: 15 September 2011

Abstract Heat and mass transfer effects on Newtonian biomagnetic fluid of blood flow through a tapered porous artery with a stenosis is investigated. Governing equations have been modeled by treating blood as Newtonian biomagnetic fluid. The governing equations are simplified under the assumption of mild stenosis. Exact solutions have been evaluated for velocity, temperature, and concentration profiles. The effects of Newtonian nature of blood on velocity, temperature, concentration profile, wall shear stress, shearing stress at the stenosis throat and impedance of the artery are discussed graphically. Stream lines have been presented in last section of the article.

Keywords Newtonian fluid · Blood flow · Tapered porous arteries · Stenosis · Analytical solution · Magnetic fluid

1 Introduction

The blood flow through a tapered arteries with a stenosis is a new area of research in fluid mechanics. Blood is a marvelous fluid which is an important factor of life. From the last few decades, the theoretical and experimental studies (Sankar and Lee 2009; Sankar and Hemalatha 2007a,b; Mekheimer and El Kot 2008; Sankar 2009; Nadeem and Akbar 2011; Akbar and Nadeem 2010; Kumar 2010) of blood flow through the circulatory system of living mammals, has been the subject of scientific research. Fluid dynamics of biological fluids in the presence of magnetic fields is biomagnetic fluid dynamics (BFD). According to BFD, which was developed by Haik et al. (1999), the biological fluids are treated as electrically

S. Nadeem (✉) · N. S. Akbar · T. Hayat
Department of Mathematics, Quaid-i-Azam University, Islamabad 45320, Pakistan
e-mail: snqau@hotmail.com

N. S. Akbar
e-mail: noreensher@yahoo.com

T. Hayat · A. A. Hendi
Department of Physics, Faculty of Science, King Saud University,
P.O.Box 1846, Riyadh 11321, Saudi Arabia

non-conducting magnetic fluids. The investigation of basic BFD flow problems attracts interest due to the numerous proposed applications in bioengineering and medical sciences. The biomagnetic (blood) fluid flow in a channel with stenosis under the influence of a steady localized magnetic field is studied by Tzirtzilakis (2008). Magneto-micropolar fluid flow, heat and mass transfer with suction and blowing through a porous medium is analyzed numerically by Elgazery (2009). Unsteady response of non-Newtonian blood flow through a stenosed artery in magnetic field was developed by Ikbal et al. (2009). Nadeem and Akbar (2011) studied the influence of heat and chemical reactions on Walter's B fluid model for blood flow through a tapered artery. The effect of heat transfer on the motion of blood in a diseased artery has been modeled under the optically thin fluid assumption was developed by Ogulu and Abbey (2005). Chakravarty and Sen (2005) studied mathematical model describing the dynamic response of heat and mass transfer in blood flow through bifurcated arteries under stenotic condition. Some important investigations related to blood flow in arteries are cited in the studies of Ai and Vafai (2006), Yang and Vafai (2006, 2008), and Khakpoura and Vafai (2008a,b).

To show the application of computational fluid dynamics in biomedical engineering, Qiao and Liu (2008) studied medical application oriented blood flow simulation. They observed that the simulation of blood flow is of great importance for understanding the function of the cardiovascular system under normal and abnormal conditions, designing cardiovascular devices, and diagnosing and treating disease. It is helpful and economical that the physician can utilize computational tools to construct and evaluate a combined anatomic/physiologic model to predict the outcome of alternative treatment plans for an individual patient. Computer assisted surgery has become a powerful assistant for the modern medical application (Nadeem et al. 2009). Some recent developments which have been made to study the biomagnetic fluid and heat transfer phenomena are cited in the studies of Nadeem and Akbar (2009a,b,c,d), Nadeem et al. (2010a,b,c).

Motivated from the above analysis, the objective of the present article is to study the heat and mass transfer effects on Newtonian biomagnetic fluid of blood flow through a tapered porous artery with a stenosis. We have developed our article as follows: In Sect. 2, we have presented the physical and mathematical formulation of the problem. In Sect. 3, we have presented the solutions to the problem in detail, while in Sect. 4, we give a quantitative discussion of the consequences of the graphical results. Trapping phenomena have also been discussed in Sect. 4.

2 Mathematical Model

Consider the continuity, the balance of momentum, temperature, and concentration for hydromagnetic fluid with porous medium

$$\operatorname{div}\mathbf{V} = \mathbf{0}. \tag{1}$$

$$\rho\frac{\mathrm{d}\mathbf{V}}{\mathrm{d}t} = -\nabla p + \operatorname{div}S + J \times H_0 + \frac{\mathbf{V}\Phi}{k_1}. \tag{2}$$

$$\rho c_p\frac{\mathrm{d}\bar{T}}{\mathrm{d}t} = k\nabla^2\bar{T} + S{\cdot}L. \tag{3}$$

$$\frac{\mathrm{d}\bar{C}}{\mathrm{d}t} = D\nabla^2\bar{C} + \frac{DK_\mathrm{T}}{T_\mathrm{m}}\nabla^2\bar{T}. \tag{4}$$

where

$$\mathbf{S} = -pI + \mu A_\mathbf{1},\ A_\mathbf{1} = L + L^t,\ L \text{ is gradient of } \mathbf{V}$$

In the above equations, $\bar{p}$ is the pressure, $\bar{T}$ is the temperature, $\bar{C}$ is the concentration of fluid (Mass of the fluid) , ρ is the density, k_1 is the permeability of the porous medium, c_p is the specific heat at constant pressure, T_{m} is the temperature of the medium, D is the coefficients of mass diffusivity, K_{T} is the thermal-diffusion ratio, $\bar{\mu}$ is the viscosity, k denotes the the thermal conductivity, and H_0 is applied magnetic field.

3 Formulation of the Problem

Consider the flow of an incompressible magnetohydrodynamic (MHD) Newtonian fluid lying in a porous arteries having length L. We are considering the cylindrical coordinate system $(r,\ \theta,\ z)$ in a such a way that $\bar{u}, \bar{v}$, and $\bar{w}$ are the velocity component in $\bar{r}, \bar{\theta}$, and $\bar{z}$ directions, respectively. The equations governing the steady incompressible MHD Newtonian fluid through porous medium in view of Eqs. 1–4 are given as

$$\frac{\partial \bar{u}}{\partial \bar{r}} + \frac{\bar{u}}{\bar{r}} + \frac{\partial \bar{w}}{\partial \bar{z}} = 0, \tag{5}$$

$$\rho\left[\bar{u}\frac{\partial \bar{u}}{\partial \bar{r}} + \bar{w}\frac{\partial \bar{u}}{\partial \bar{r}}\right] = -\frac{\partial \bar{p}}{\partial \bar{r}} + \frac{\partial}{\partial \bar{r}}\left[2\mu\frac{\partial \bar{u}}{\partial \bar{r}}\right] + \frac{2\mu}{\bar{r}}\left(\frac{\partial \bar{u}}{\partial \bar{r}} - \frac{\bar{u}}{\bar{r}}\right) + \frac{\partial}{\partial \bar{z}}\left[\mu\left(\frac{\partial \bar{u}}{\partial \bar{z}} + \frac{\partial \bar{w}}{\partial \bar{r}}\right)\right] \tag{6}$$

$$\rho\left[\bar{u}\frac{\partial \bar{w}}{\partial \bar{r}} + \bar{w}\frac{\partial \bar{w}}{\partial \bar{z}}\right] = -\frac{\partial \bar{p}}{\partial \bar{z}} + \frac{\partial}{\partial \bar{z}}\left[2\mu\frac{\partial \bar{w}}{\partial \bar{z}}\right] + \frac{1}{\bar{r}}\frac{\partial}{\partial \bar{r}}\left[\mu\bar{r}\left(\frac{\partial \bar{u}}{\partial \bar{z}} + \frac{\partial \bar{w}}{\partial \bar{r}}\right)\right] - \sigma_1\mu_{\mathrm{m}}^2 H_0^2\bar{w} - \frac{\mu\bar{w}}{k_1}, \tag{7}$$

$$\rho c_p\left[\bar{u}\frac{\partial \bar{T}}{\partial \bar{r}} + \bar{w}\frac{\partial \bar{T}}{\partial \bar{z}}\right] = \frac{k}{\bar{r}}\frac{\partial}{\partial \bar{r}}\left(\bar{r}\frac{\partial \bar{T}}{\partial \bar{r}}\right) + \left(\frac{\partial \bar{w}}{\partial \bar{r}}\right)^2. \tag{8}$$

$$\left(\bar{u}\frac{\partial}{\partial \bar{r}} + \bar{w}\frac{\partial}{\partial \bar{z}}\right)\bar{C} = D\left(\frac{\partial^2 \bar{C}}{\partial \bar{r}^2} + \frac{1}{\bar{r}}\frac{\partial \bar{C}}{\partial \bar{r}} + \frac{\partial^2 \bar{C}}{\partial \bar{z}^2}\right) + \frac{DK_{\mathrm{T}}}{T_{\mathrm{m}}}\left(\frac{\partial^2 \bar{T}}{\partial \bar{r}^2} + \frac{1}{\bar{r}}\frac{\partial \bar{T}}{\partial \bar{r}} + \frac{\partial^2 \bar{T}}{\partial \bar{z}^2}\right). \tag{9}$$

where σ_1 is the electrical conductivity, μ_{m} is the magnetic permeability. $\bar{u}, \bar{w}$ are the respective velocity components in the radial and axial directions.

The geometry of the stenosis is defined as Mekheimer and El Kot (2008).

$$\begin{aligned} h(z) &= d(z)\left[1 - \eta\left(b^{n-1}(z-a) - (z-a)^n\right)\right], \\ a &\le z \le a + b, \\ &= d(z), \quad \text{otherwise} \end{aligned} \tag{10}$$

with

$$d(z) = d_0 + \xi z,$$

in which $d(z)$ is the radius of the tapered arterial segment in the stenotic region, d_0 is the radius of the non-tapered artery in the non-stenotic region, ξ is the tapering parameter, b is the length of stenosis, $(n \ge 2)$ is a parameter determining the shape of the constriction profile and referred to as the shape parameter (the symmetric stenosis occurs for $n = 2$), and a indicates its location as shown in Fig. 1. The parameter η is defined as

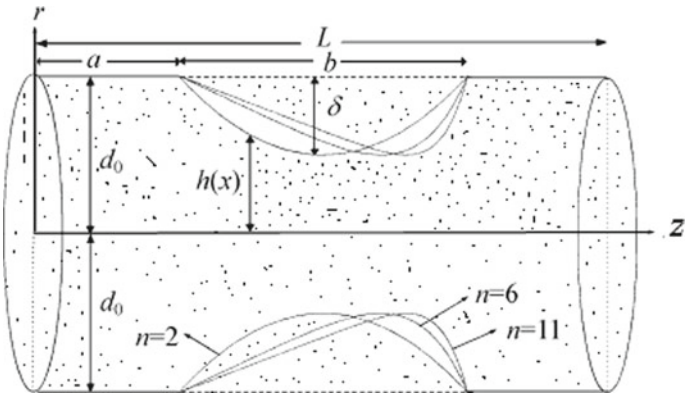

Fig. 1 Geometry of an axially nonsymmetric stenosis in a porous artery

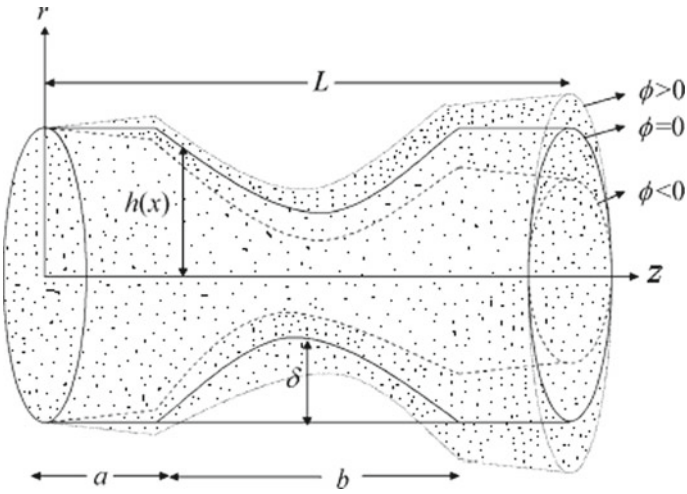

Fig. 2 Geometry of the stenosed tapered porous artery for different taper angle

$$\eta = \frac{\delta n^{\frac{n}{n-1}}}{d_0 b^n (n-1)}, \tag{11}$$

where δ denotes the maximum height of the stenosis located at

$$z = a + \frac{b}{n^{\frac{n}{n-1}}}.$$

We introduce the non-dimensional variables

$$r = \frac{\bar{r}}{d_0},\ z = \frac{\bar{z}}{b},\ w = \frac{\bar{w}}{u_0},\ u = \frac{b\bar{u}}{u_0\delta},\ p = \frac{d_0^2\bar{p}}{u_0 b\mu},\ h = \frac{\bar{h}}{d_0},$$
$$Re = \frac{\rho b u_0}{\mu},\ \theta = \frac{\left(\bar{T} - \bar{T}_0\right)}{\bar{T}_0},\ Pr = \frac{\mu c_p}{k},\ E_c = \frac{u_0^2}{c_p\left(T_0 - T_1\right)},$$
$$Z = \frac{k_1}{d_0},\ M = \sigma_1\mu_{\mathrm{m}}H_0\sqrt{\frac{\sigma_1}{\mu}}. \tag{12}$$

here u_0 is the velocity averaged over the section of the tube of the width d_0. M is magnetic field.

Making use of Eq. 12 and after adopting the additional conditions (Mekheimer and El Kot 2008),

$$(i)\ \frac{Re\delta^* n^{\left(\frac{1}{n-1}\right)}}{b} << 1, \tag{13}$$

$$(ii)\ \frac{d_0 n^{\left(\frac{1}{n-1}\right)}}{b} \sim O(1), \tag{14}$$

Equations 5–9, for the case of mild stenosis $\left(\frac{\delta^*}{d_0} << 1\right)$, take the form

$$\frac{\partial u}{\partial r} + \frac{u}{r} + \frac{\partial w}{\partial z} = 0, \tag{15}$$

$$\frac{\partial p}{\partial r} = 0, \tag{16}$$

$$\frac{\partial p}{\partial z} = \frac{1}{r}\frac{\partial}{\partial r}\left[r\left(\frac{\partial w}{\partial r}\right)\right] - \left(M^2 + \frac{1}{Z}\right)w. \tag{17}$$

$$0 = \frac{1}{r}\frac{\partial}{\partial r}\left[r\left(\frac{\partial \theta}{\partial r}\right)\right] + E_c Pr\left(\left(\frac{\partial w}{\partial r}\right)^2\right) \tag{18}$$

$$\frac{1}{S_c}\left(\frac{1}{r}\frac{\partial}{\partial r}\left(r\frac{\partial \sigma}{\partial r}\right)\right) + S_r\left(\frac{1}{r}\frac{\partial}{\partial r}\left(r\frac{\partial \theta}{\partial r}\right)\right) = 0, \tag{19}$$

where $B_r = E_c Pr$.

The corresponding boundary conditions are

$$\frac{\partial w}{\partial r} = 0,\ \frac{\partial \theta}{\partial r} = 0,\ \frac{\partial \sigma}{\partial r} = 0 \ \text{at}\ r = 0, \tag{20a}$$

$$w = 0,\ \theta = 0,\ \sigma = 0 \ \text{at}\ r = h(z), \tag{20b}$$

in which

$$h(z) = (1 + \xi z)\left[1 - \eta_1\left((z - \sigma_2) - (z - \sigma_2)^n\right)\right],$$
$$\sigma_2 \le z \le \sigma_2 + 1, \tag{21}$$

and

$$\eta_1 = \frac{\delta n^{\frac{n}{n-1}}}{(n-1)},\ \delta = \frac{\delta^*}{d_0},\ \sigma = \frac{a}{b},\ \xi' = \frac{\xi b}{d_0}$$

where $(\xi = \tan\phi)$, ϕ is called tapered angle and for converging tapering $(\phi < 0)$, non-tapered artery $(\phi = 0)$ and the diverging tapering $(\phi > 0)$ as discussed in Mekheimer and El Kot (2008) (Fig. 2).

4 Solution of the Problem

4.1 Exact Solution

Expression for velocity field, temperature and concentration field, and pressure gradient can be written as

$$w\,(r,z) = \frac{\mathrm{d}p}{\mathrm{d}z}\frac{1}{\left(M^2+\frac{1}{Z}\right)}\frac{\left(I_0\left(\sqrt{\left(M^2+\frac{1}{Z}\right)}r\right)-I_0\left(\sqrt{\left(M^2+\frac{1}{Z}\right)}h\right)\right)}{I_0\left(\sqrt{\left(M^2+\frac{1}{Z}\right)}h\right)}, \tag{22}$$

$$\theta\,(r,z) = -B_r\left(\frac{\partial p}{\partial z}\right)^2\frac{1}{\left(M^2+\frac{1}{Z}\right)^2\left(I_0\left(\sqrt{\left(M^2+\frac{1}{Z}\right)}h\right)\right)^2}\sum_{k,m=0}^{\infty}a_{mk} \times\left(\left(\sqrt{\left(M^2+\frac{1}{Z}\right)}r\right)^{2k+2m+4}-\left(\sqrt{\left(M^2+\frac{1}{Z}\right)}h\right)^{2k+2m+4}\right), \tag{23}$$

$$\sigma\,(r,z) = S_rS_cB_r\left(\frac{\partial p}{\partial z}\right)^2\frac{1}{\left(M^2+\frac{1}{Z}\right)^2\left(I_0\left(\sqrt{\left(M^2+\frac{1}{Z}\right)}h\right)\right)^2}\sum_{k,m=0}^{\infty}a_{mk} \times\left(\left(\sqrt{\left(M^2+\frac{1}{Z}\right)}r\right)^{2k+2m+4}-\left(\sqrt{\left(M^2+\frac{1}{Z}\right)}h\right)^{2k+2m+4}\right), \tag{24}$$

$$\frac{\mathrm{d}p}{\mathrm{d}z} = \frac{2M^4I_0\left(\sqrt{\left(M^2+\frac{1}{Z}\right)}h\right)Q}{2\sqrt{\left(M^2+\frac{1}{Z}\right)}hI_1\left(\sqrt{\left(M^2+\frac{1}{Z}\right)}h\right)-\left(M^2+\frac{1}{Z}\right)h^2I_0\left(\sqrt{\left(M^2+\frac{1}{Z}\right)}h\right)}, \tag{25}$$

The pressure drop ($\Delta p = p$ at $z = 0$ and $\Delta p = -p$ at $z = L$) across the stenosis between the section $z = 0$ and $z = L$ is obtain from (26) as done by Mekheimer and El Kot (2008)

$$\Delta p = \int_0^L\left(-\frac{\mathrm{d}p}{\mathrm{d}z}\right)\mathrm{d}z. \tag{26}$$

4.2 Resistance Impedance

The resistance impedance (resistance to blood flow) is obtain from Eq. 27 as

$$\bar{\lambda} = \frac{\Delta p}{F} = 8\left\{\int_0^a F\,(z)|_{h=1}\,\mathrm{d}z + \int_a^{a+b}F\,(z)\,\mathrm{d}z + \int_{a+b}^{L}F\,(z)|_{h=1}\,\mathrm{d}z\right\} \tag{27}$$

where

$$F\,(z) = \frac{-M^4I_0\left(\sqrt{\left(M^2+\frac{1}{Z}\right)}h\right)}{4\left(2\sqrt{\left(M^2+\frac{1}{Z}\right)}hI_1\left(\sqrt{\left(M^2+\frac{1}{Z}\right)}h\right)-\left(M^2+\frac{1}{Z}\right)h^2I_0\left(\sqrt{\left(M^2+\frac{1}{Z}\right)}h\right)\right)},$$

Table 1 Comparison of our results with previous work when $\delta = 0.025, \sigma = 0.00,$ $F = 0.3, z = 0.1, n = 2.$

r	$M = 0, Z = 0$ our results	$N = 0$[a]	$\alpha = 0$[b]	$\lambda_1 = 0$[c]
−1.0	0.000	0.000	0.000	0.000
−0.8	0.303	0.305	0.116	0.116
−0.6	0.535	0.537	0.204	0.204
−0.4	0.703	0.701	0.416	0.416
−0.2	0.802	0.803	0.533	0.533
0.0	0.000	0.000	0.000	0.000
0.2	0.802	0.803	0.533	0.533
0.4	0.703	0.701	0.416	0.416
0.6	0.535	0.537	0.204	0.204
0.8	0.303	0.305	0.116	0.116
1.0	0.000	0.000	0.000	0.000

[a] Mekheimer and El Kot (2008)
[b] Nadeem and Akbar (2011)
[c] Akbar and Nadeem (2010)

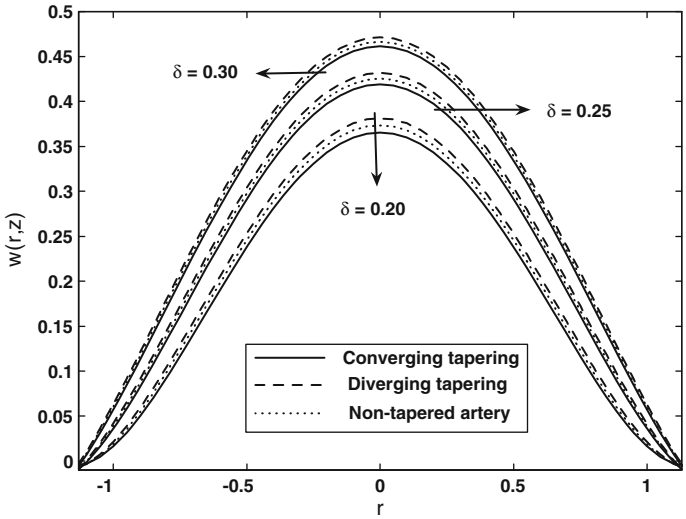

Fig. 3 Variation of velocity profile for $F = 0.3, M = 0.2, Z = 2, n = 2, z = 0.95, \sigma = 0.00$

so, the resistance impedance is

$$\tilde{\lambda} = 8\left\{(L-b)\left(\frac{-M^4 I_0\left(\sqrt{\left(M^2+\frac{1}{Z}\right)}\right)}{4\left(2MI_1\left(\sqrt{\left(M^2+\frac{1}{Z}\right)}\right)-(M)^2 I_0\left(\sqrt{\left(M^2+\frac{1}{Z}\right)}\right)\right)}\right)+\int_a^{a+b} F(z)\,\mathrm{d}z\right\}, \tag{28}$$

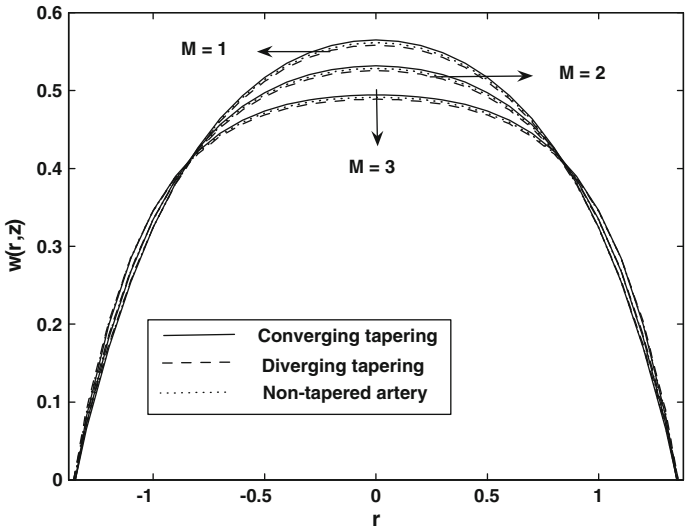

Fig. 4 Variation of velocity profile for $F = 0.3, \delta = 0.9, Z = 0.5, n = 2, z = 0.5, \sigma = 0.00$

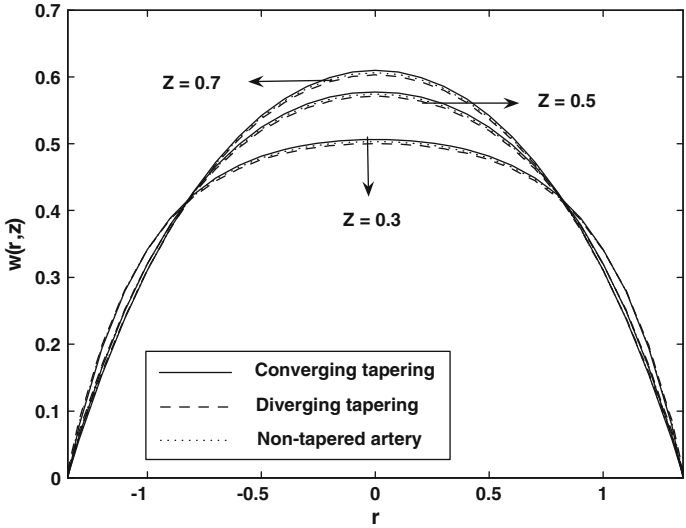

Fig. 5 Variation of velocity profile for $F = 0.3, \delta = 0.9, M = 0.2, n = 2, z = 0.5, \sigma = 0.00$

4.3 Expression for the Wall Shear Stress

The nonzero dimensionless shear stress is given by

$$\tilde{S}_{rz} = \left[\left(\frac{\partial w}{\partial r}\right)\right], \tag{29}$$

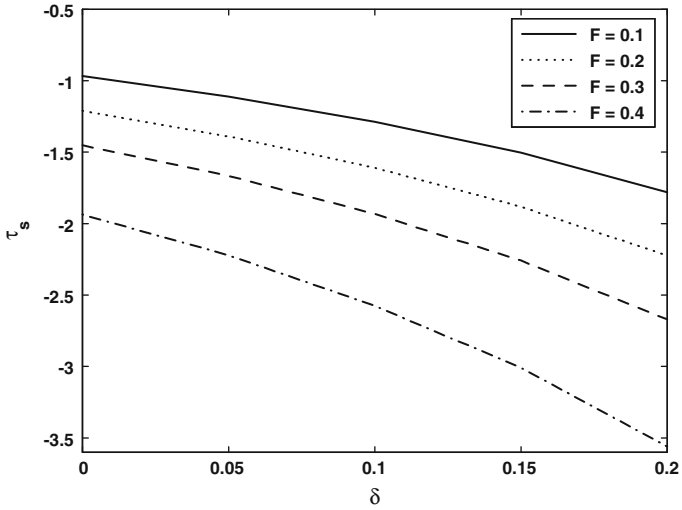

Fig. 6 Variation of shear stress at the stenosis throat for $Z = 0.8$, $M = 2$

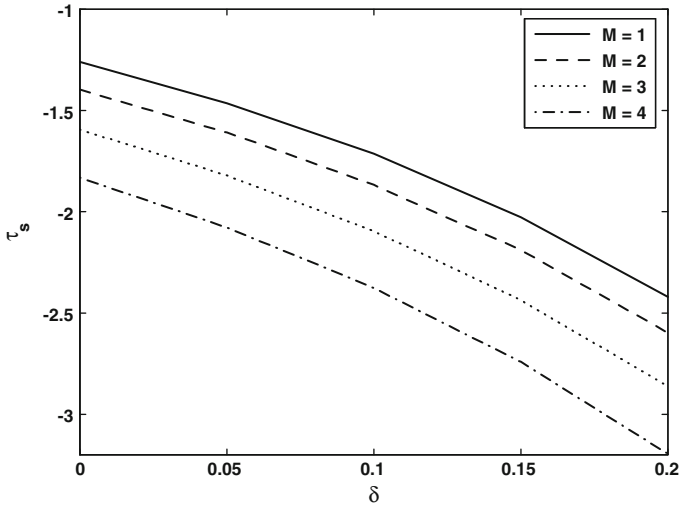

Fig. 7 Variation of shear stress at the stenosis throat for $Z = 0.8$, $F = 0.3$

From Eq. 29, we can find the expression for wall shear stress by

$$\tilde{S}_{rz} = \left[\left(\frac{\partial w}{\partial r}\right)\right]\Big|_{r=h}, \tag{30}$$

So

$$\tilde{S}_{rz} = \frac{2M^3 F I_1\left(\sqrt{(M^2+\frac{1}{Z})}h\right)}{2\left(\sqrt{(M^2+\frac{1}{Z})}h\right) I_1\left(\sqrt{(M^2+\frac{1}{Z})}h\right) - (M^2+\frac{1}{Z})\, h^2 I_0\left(\sqrt{(M^2+\frac{1}{Z})}h\right)}, \tag{31}$$

where F is the flow rate.

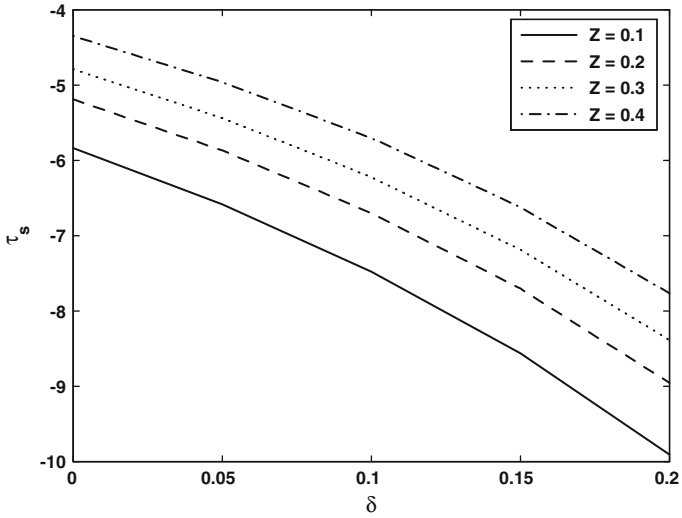

Fig. 8 Variation of shear stress at the stenosis throat for $M = 2$, $F = 0.3$

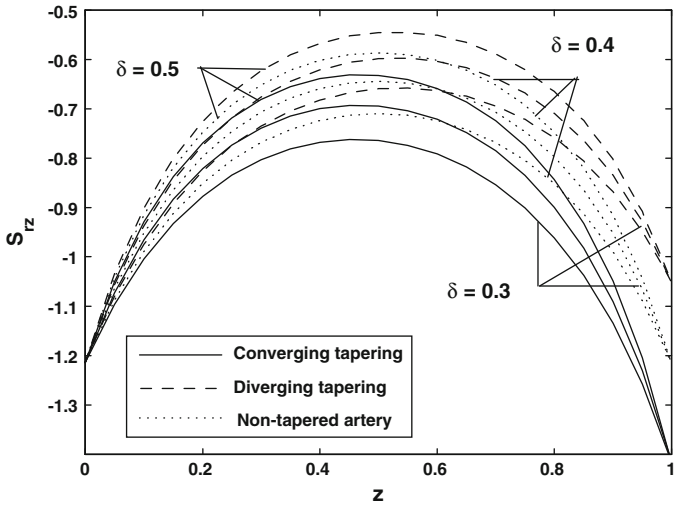

Fig. 9 Variation of wall shear stress for $M = 0.2$, $F = 0.3$, $n = 2$, $\sigma = 0.0$, $Z = 2$

We can note that the shearing stress at the stenosis throat, i.e., the wall shear at the maximum height of the stenosis located at $z = \frac{a}{b} + \frac{1}{n^{\frac{n}{n-1}}}$, i.e.,

$$\tilde{\tau}_{\mathrm{s}} = \tilde{S}_{rz}\Big|_{h=1-\delta} \tag{32}$$

We can find the final expression for the dimensionless resistance to λ, wall shear stress S_{rz} and the shearing stress at the throat τ_{s} by

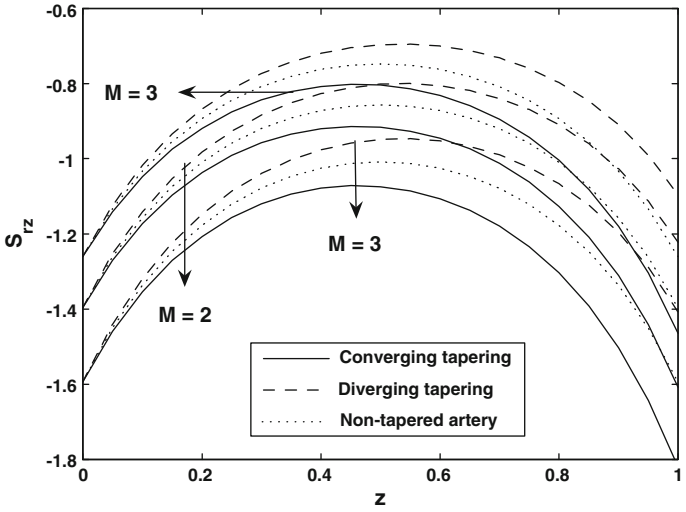

Fig. 10 Variation of wall shear stress for $\delta = 0.5$, $F = 0.3$, $n = 2$, $\sigma = 0.0$, $Z = 2$

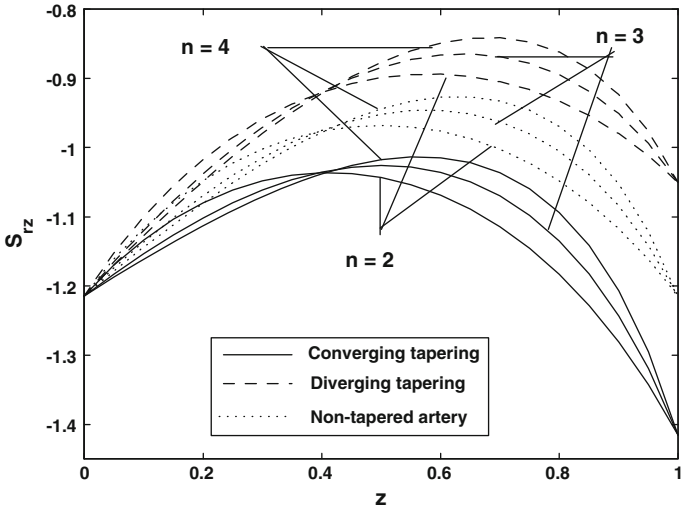

Fig. 11 Variation of wall shear stress for $\delta = 0.2$, $F = 0.3$, $M = 0.2$, $\sigma = 0.0$, $Z = 2$

$$\lambda = \frac{8}{3}\left\{\left(1-\frac{b}{L}\right)\left(\frac{-M^4 I_0\left(\sqrt{\left(M^2+\frac{1}{Z}\right)}\right)}{4\left(2\sqrt{\left(M^2+\frac{1}{Z}\right)}I_1\left(\sqrt{\left(M^2+\frac{1}{Z}\right)}\right)-\left(M^2+\frac{1}{Z}\right)I_0\left(\sqrt{\left(M^2+\frac{1}{Z}\right)}\right)\right)}\right) + \frac{1}{L}\int_a^{a+b} F(z)\,\mathrm{d}z\right\}, \tag{33}$$

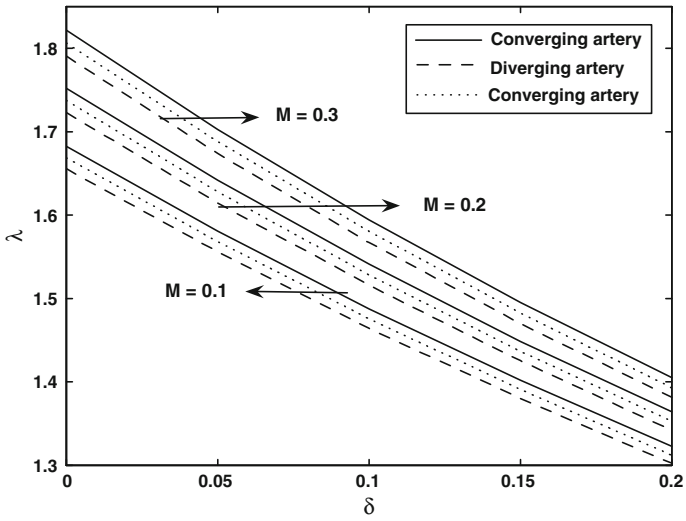

Fig. 12 Variation of resistance impedance for $n = 2$, $F = 0.3$, $L = 1$, $\sigma = 0.0$, $b = 1$, $Z = 2$

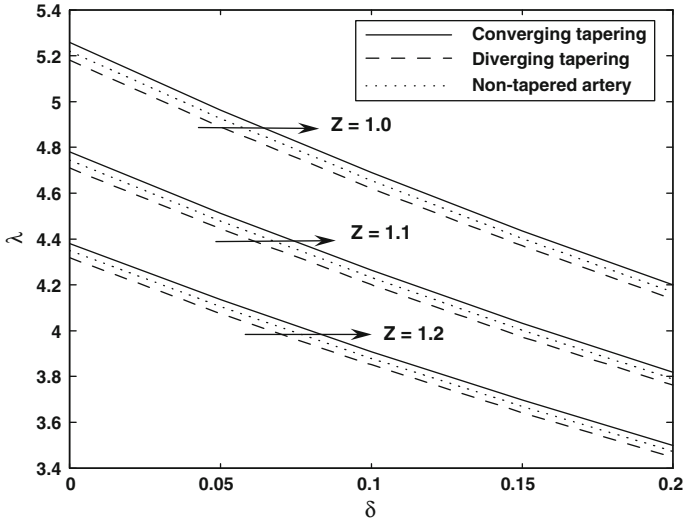

Fig. 13 Variation of impedance resistance for $n = 2$, $F = 0.3$, $L = 1$, $\sigma = 0.0$, $b = 1$, $M = 2$

$$S_{rz} = \frac{M^3 I_1\left(\sqrt{(M^2+\frac{1}{Z})}h\right)}{2\left(2\left(\sqrt{(M^2+\frac{1}{Z})}h\right) I_1\left(\sqrt{(M^2+\frac{1}{Z})}h\right) - (M^2+\frac{1}{Z})\,h^2 I_0\left(\sqrt{(M^2+\frac{1}{Z})}h\right)\right)}, \tag{34}$$

$$\tau_s = \left.\frac{M^3 I_1\left(\sqrt{(M^2+\frac{1}{Z})}h\right)}{2\left(2\left(\sqrt{(M^2+\frac{1}{Z})}h\right) I_1\left(\sqrt{(M^2+\frac{1}{Z})}h\right) - (M^2+\frac{1}{Z})\,h^2 I_0\left(\sqrt{(M^2+\frac{1}{Z})}h\right)\right)}\right|_{h=1-\delta}, \tag{35}$$

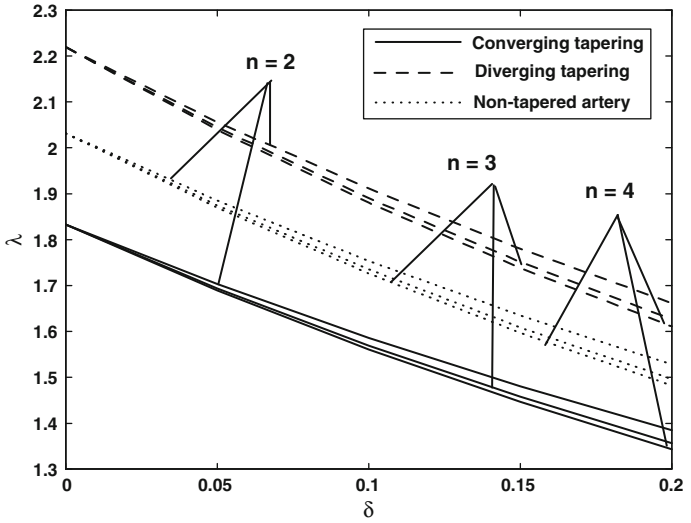

Fig. 14 Variation of impedance resistance for $Z = 2$, $F = 0.3$, $L = 1$, $\sigma = 0.0$, $b = 1$, $M = 2$

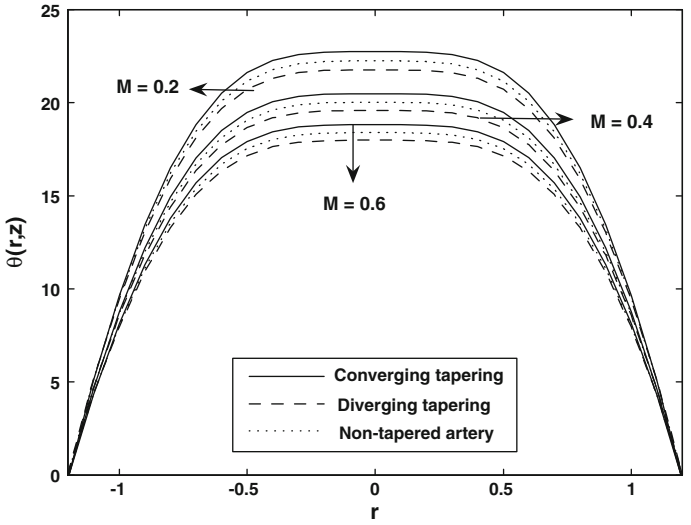

Fig. 15 Variation of temperature profile for $z = 0.5$, $F = 0.3$, $n = 2$, $\sigma = 0.0$, $B_r = 0.45$, $\delta = 0.6$, $Z = 2$

where

$$\lambda = \frac{\tilde{\lambda}}{\lambda_0},\ S_{rz} = \frac{\tilde{S}_{rz}}{\tau_0},\ \tau_s = \frac{\tilde{\tau}_s}{\tau_0},\ \lambda_0 = 3L,\ \tau_0 = 4F.$$

and λ_0, τ_0 are the resistance to flow and the wall shear stress for a flow in a normal artery (no stenosis).

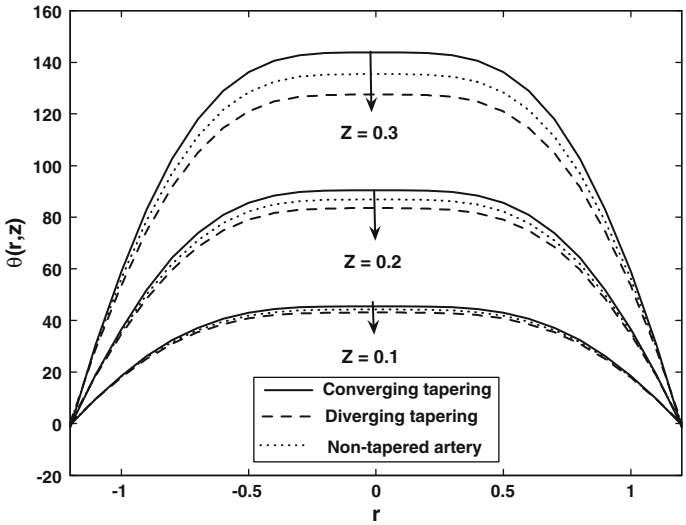

Fig. 16 Variation of temperature profile for $z = 0.5$, $F = 0.3$, $n = 2$, $\sigma = 0.0$, $B_r = 0.45$, $\delta = 0.6$, $M = 2$

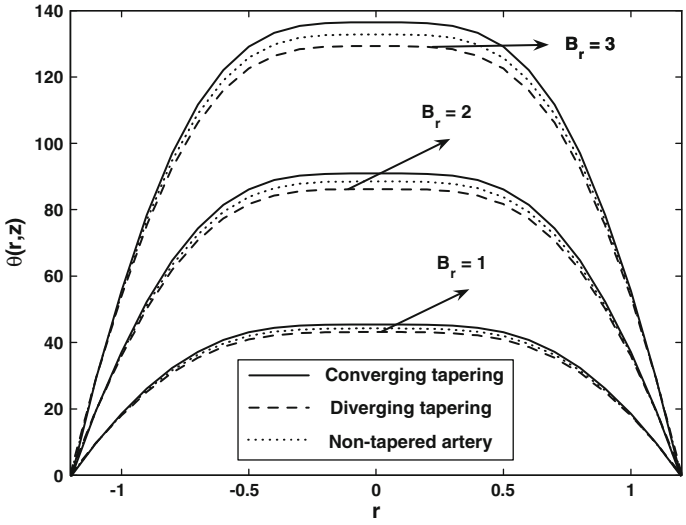

Fig. 17 Variation of temperature profile for $z = 0.5$, $F = 0.3$, $n = 2$, $\sigma = 0.0$, $Z = 0.45$, $\delta = 0.6$, $M = 2$

4.4 Comparison of our Results with Previous Work

Table 1 shows the comparison of our results with previous work when $\delta = 0.025, \sigma = 0.00$, $F = 0.3$, $z = 0.1$, $n = 2$..

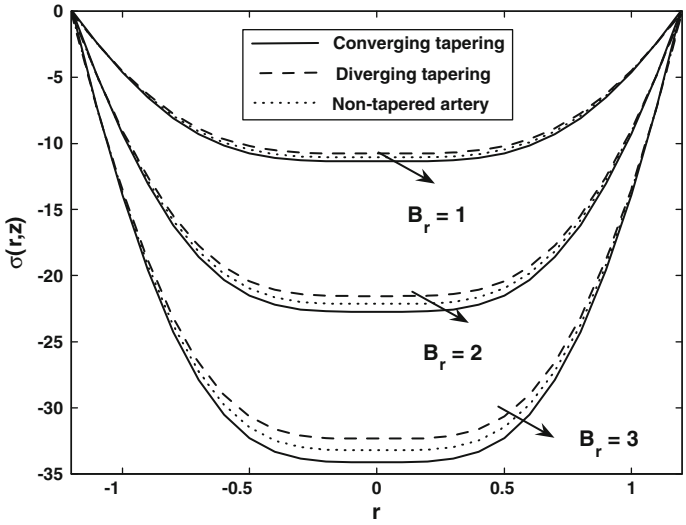

Fig. 18 Variation of concentration profile for $z = 0.5$, $F = 0.3$, $n = 2$, $\sigma = 0.0$, $Z = 0.45$, $\delta = 0.6$, $M = 2$, $S_r = 0.5$, $S_c = 0.5$

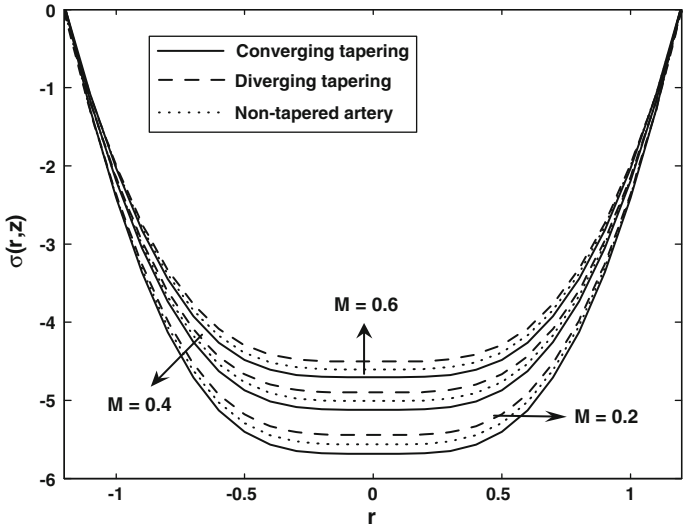

Fig. 19 Variation of concentration profile for $z = 0.5$, $F = 0.3$, $n = 2$, $\sigma = 0.0$, $B_r = 0.45$, $\delta = 0.6$, $Z = 2$, $S_r = 0.5$, $S_c = 0.5$

5 Numerical Results and Discussion

The quantitative effects of the magnetic field M, porosity parameter Z, the stenosis shape n, and maximum height of the stenosis δ for converging tapering, diverging tapering, and non-tapered arteries for Newtonian fluid are observed physically through Figs. 3, 4, 5, 6, 7, 8, 9, 10, 11, 12, 13, 14, 15, and 16. The variation of axial velocity for M, W, and δ for the case of converging tapering, diverging tapering and non-tapered arteries are displayed in

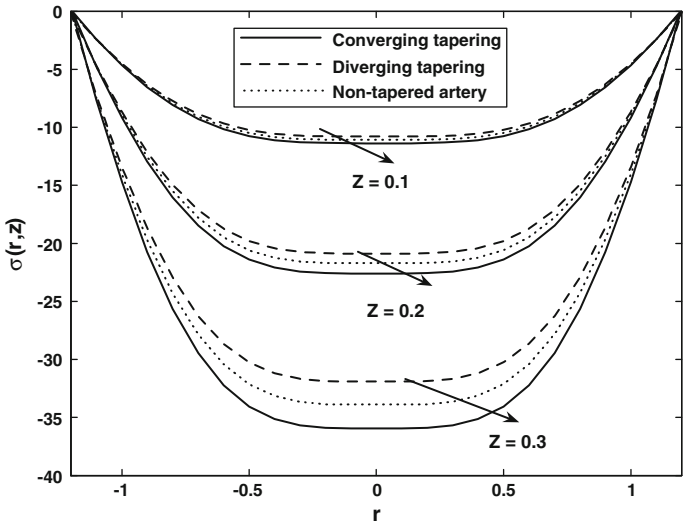

Fig. 20 Variation of concentration profile for $z = 0.5$, $F = 0.3$, $n = 2$, $\sigma = 0.0$, $B_r = 0.45$, $\delta = 0.6$, $M = 2$, $S_r = 0.5$, $S_c = 0.5$

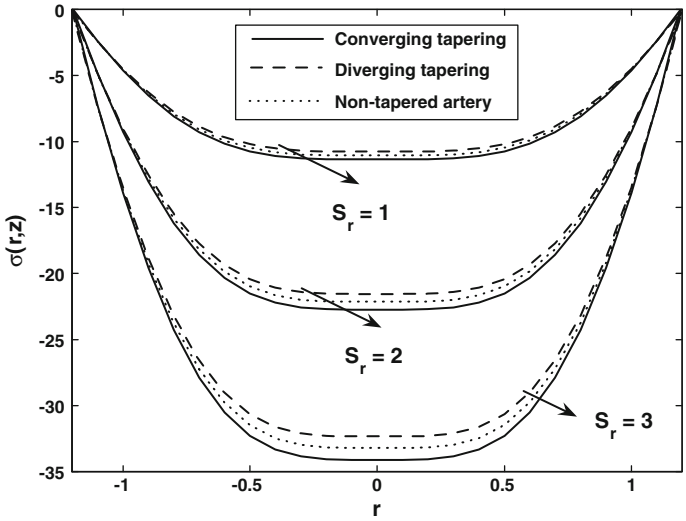

Fig. 21 Variation of concentration profile for $z = 0.5$, $F = 0.3$, $n = 2$, $\sigma = 0.0$, $B_r = 0.45$, $\delta = 0.6$, $M = 2$, $Z = 0.5$, $S_c = 0.5$

Figs. 3, 4, and 5. In Figs. 3, 4, and 5, we observed that with an increase in M, δ, and velocity profile decreases, while increases with an increase in Z. It is also seen that for the case of converging tapering velocity gives larger values as compared with the case of diverging tapering and non-tapered arteries. Figures 6, 7, and 8 are prepared to see the variation of the shearing stress at the stenosis throat τ_s with δ. It is analyzed through figures that shearing stress at the stenosis throat decreases with an increase in F and M, while increases with an increase in Z. Figures 9, 10, and 11 shows how the converging tapering, diverging tapering,

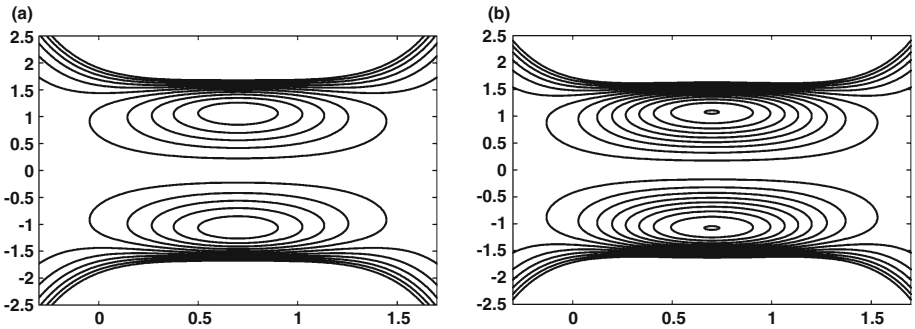

Fig. 22 Stream lines for different values of n: **a** $n = 2$, **b** $n = 4$. Other parameters are $\phi = \pi$, $M = 1$, $\delta = 0.01$, $\sigma = 0.4$, $Z = 0.3$, $F = 0.2$

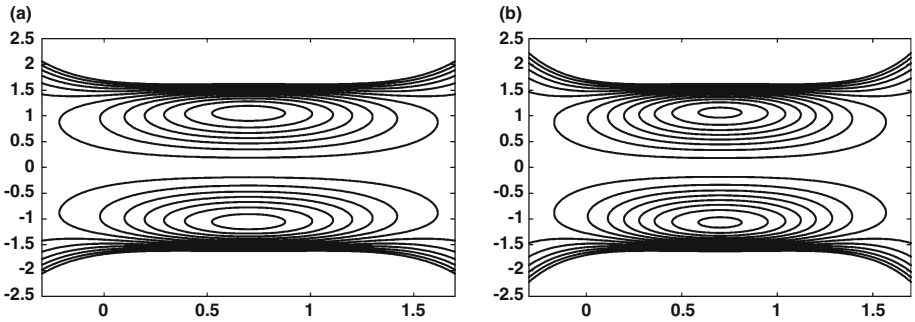

Fig. 23 Stream lines for different values of M: **a** $M = 2$, **b** $M = 4$. Other parameters are $\phi = \pi$, $n = 2$, $\delta = 0.01$, $\sigma = 0.4$, $Z = 0.3$, $F = 0.2$

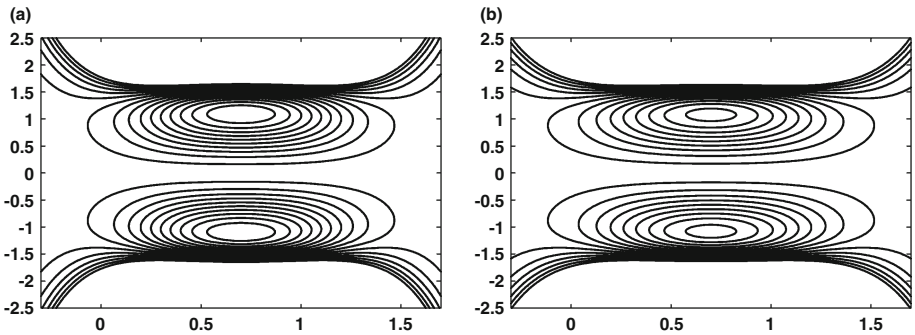

Fig. 24 Stream lines for different values of Z: **a** $Z = 0.2$, **b** $Z = 0.4$. Other parameters are $\phi = \pi$, $n = 2$, $\delta = 0.01$, $\sigma = 0.4$, $M = 3$, $F = 0.2$

and non-tapered arteries influence on the wall shear stress S_{rz}. It is observed that with an increase in δ, M and n shear stress increases, the stress yield diverging tapering with tapered angle $\phi > 0$, converging tapering with tapered angle $\phi < 0$, and non-tapered artery with tapered angle $\phi = 0$. In Figs. 12, 13, and 14, we notice that the impedance resistance increases for converging tapering, diverging tapering, and non-tapered arteries when we increase M and m, while decreases when we increase Z. We also observed that resistive impedance in a

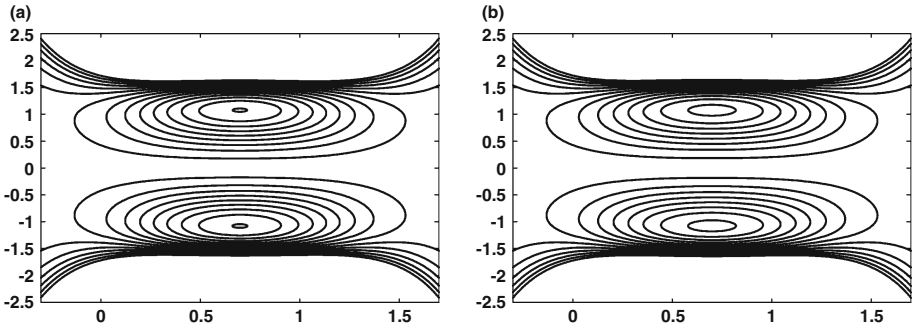

Fig. 25 Stream lines for different values of δ: **a** $\delta = 0.3$, **b** $\delta = 0.4$. Other parameters are $\phi = \pi, n = 2, Z = 0.1, \sigma = 0.4, M = 3, F = 0.2$

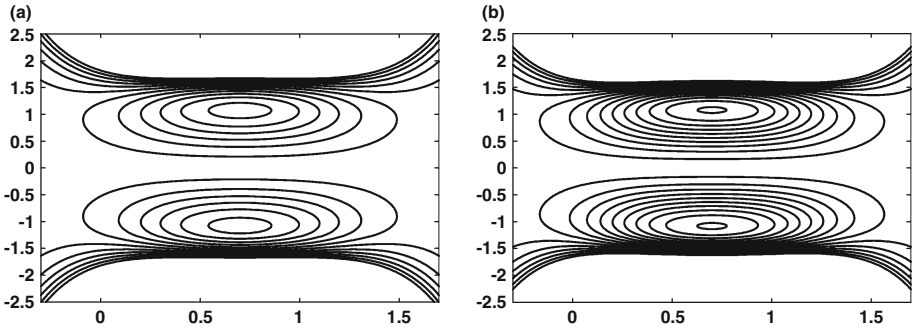

Fig. 26 Stream lines for different values of F: **a** $F = 0.3$, **b** $F = 0.4$. Other parameters are $\phi = \pi, n = 2, Z = 0.1, \sigma = 0.4, M = 3, \delta = 0.2$

diverging tapering appear to be smaller than those in converging tapering because the flow rate is higher in the former than that in the latter, as anticipated and impedance resistance attains its maximum values in the symmetric stenosis case ($n = 2$). Figures 15, 16, and 17 shows the variation of temperature profile for different values of Brickmann number B_r, magnetic field M, and porosity parameter Z. It is observed that with an increase in Brickmann number B_r and porosity parameter Z, temperature profile increases, while temperature profile decreases with an increase in magnetic field M and temperature profile gives the large values for converging tapering as compared with the diverging and non-tapered artery. Figures 18, 19, 20, and 21 are prepared to see the variation of concentration profile for Brickmann number B_r, magnetic field M, porosity parameter Z, and Soret number S_r. It is analyzed that with an increase in Brickmann number B_r, porosity parameter Z and Soret number S_r concentration profile decreases, while increases with an increase in magnetic field M. It is also observed that concentration profile has an opposite behavior as compared with the temperature profile. Trapping phenomena have been discussed in Figs. 22, 23, 24, and 25. Figures 22, 23, and 24 shows the stream lines for different values of the stenosis shape n, magnetic field M, and porosity parameter Z. It is observed that with an increase in nM and Z, number of the trapping bolus increases while size of the trapping bolus decreases. Stream lines for different values of the height of the stenosis δ are prepared in Fig. 25. It is analyzed that the size of the trapping bolus increases and number of trapping bolus decreases when we increase the height of the stenosis. Figure 26 is plotted to see the stream lines for different

values of flow rate F. It is seen that the size of the trapping bolus increases, while number of trapping bolus decreases with an increases of the flow rate F.

Acknowledgment The third author (as a visiting Professor) gratefully appreciates the support of Kind Saud University for the support (KSU-VPP-103).

References

Ai, L., Vafai, K.: A coupling model for macromolecule transport in a stenosed arterial wall. Int. J. Heat Mass Transf. **49**, 1568–1591 (2006)

Akbar, N.S., Nadeem, S.: Simulation of heat and chemical reactions on Reiner Rivlin fluid model for blood flow through a tapered artery with a stenosis. Heat Mass Transf. **46**, 531–539 (2010)

Chakravarty, S., Sen, S.: Dynamic response of heat and mass transfer in blood flow through stenosed bifurcated arteries. Korea-Aust. Rheol. J. **17**, 47–62 (2005)

Elgazery, N.S.: The effects of chemical reaction, Hall and ion-slip currents on MHD flow with temperature dependent viscosity and thermal diffusivity. Commun. Nonlinear Sci. Numer. Simul. **14**, 1267–1283 (2009)

Haik, Y., Pai, V., Chen, C.J.: Biomagnetic fluid dynamics. In: Shyy, W., Narayanan, R. (eds.) Fluid Dynamics at Interfaces, pp. 439–452. Cambridge University Press, Cambridge (1999)

Ikbal, Md.A., Chakravarty, S., Wongb, K.K.L., Mazumdar, J., Mandal, P.K.: Unsteady response of non-Newtonian blood flow through a stenosed artery in magnetic field. J. Comput. Appl. Math. **230**, 243–259 (2009)

Khakpoura, M., Vafai, K.: Effects of gender-related geometrical characteristics of aorta–iliac bifurcation on hemodynamics and macromolecule concentration distribution. Int. J. Heat Mass Transf. **51**, 5542–5551 (2008a)

Khakpoura, M., Vafai, K.: A comprehensive analytical solution of macromolecular transport within an artery. Int. J. Heat Mass Transf. **51**, 2905–2913 (2008b)

Kumar, A.: Mathematical Model of Blood Flow in Arteries with Porous Effects, IFMBE Proceeding (2010)

Mekheimer, Kh. S., El Kot, M.A.: The micropolar fluid model for blood flow through a tapered artery with a stenosis. Acta Mech. Sin. **24**, 637–644 (2008)

Nadeem, S., Akbar, N.S.: Influence of heat transfer on a peristaltic transport of Herschel–Bulkleyfluid in a non-uniform inclined tube. Commun. Nonlinear Sci. Numer. Simul. **14**, 4100–4113 (2009a)

Nadeem, S., Akbar, N.S.: Peristaltic Flow of a Jeffrey Fluid with Variable Viscosity in an Asymmetric Channel. Z. Naturforsch **64a**, 713–722 (2009b)

Nadeem, S., Akbar, N.S.: Influence of heat transfer on a peristaltic flow of Johnson Segalman fluid in a non uniform tube. Int. Commun. Heat Mass Transf. **36**, 1050–1059 (2009c)

Nadeem, S., Akbar, N.S.: Effects of heat transfer on the peristaltic transport of MHD Newtonian fluid with variable viscosity: application of Adomian decomposition method. Commun. Nonlinear Sci. Numer. Simul. **14**, 3844–3855 (2009d)

Nadeem, S., Hayat, T., Akbar, N.S., Malik, M.Y.: On the influence of heat transfer in peristalsis with variable viscosity. Int. J. Heat Mass Transf. **52**, 4722–4730 (2009)

Nadeem, S., Akbar, N.S., Hameed, M.: Peristaltic transport and heat transfer of a MHD Newtonian fluid with variable viscosity. Int. J. Numer. Methods Fluids **63**, 1375–1393 (2010a)

Nadeem, S., Akbar, N.S., Malik, M.Y.: Exact and Numerical Solutions of a Micropolar Fluid in a Vertical Annulus. Numer. Methods Partial Diff. Equ. **26**, 1660–1674 (2010b)

Nadeem, S., Akbar, N.S., Malik, M.Y.: Numerical solutions of peristaltic flow of a Newtonian fluid under the effects of magnetic field and heat transfer in a porous concentric tubes. Zeitschrift Fur Naturforschung **65**, 369–380 (2010c)

Nadeem, S., Akbar, N.S.: Influence of heat and chemical reactions on Walter's B fluid model for blood flow through a tapered artery. J. Taiwan Inst. Chem. Eng. **42**, 67–75 (2011)

Ogulu, A., Abbey, T.M.: Simulation of heat transfer on an oscillatory blood flow in an indented porous artery. Int. Commun. Heat Mass Transf. **32**, 983–989 (2005)

Qiao, A., Liu, Y.: Medical application oriented blood flow simulation. Clin. Biomech. **23**, S130–S136 (2008)

Sankar, D.S.: A two-fluid model for pulsatile flow in catheterized blood vessels. Int. J. Non-Lin Mech. **44**, 337–351 (2009)

Sankar, D.S., Hemalatha, K.: A non-Newtonian fluid flow model for blood flow through a catherized artery. Appl. Math Model **31**, 1847–1864 (2007a)

Sankar, D.S., Hemalatha, K.: Pulsatile flow of Herschel–Bulkley fluid for blood flow through a catheterized artery-a mathematical model. Appl. Math. Model **31**, 1497–1517 (2007b)

Sankar, D.S., Lee, U.: Mathematical modelling of pulsatile flow of non-Newtonian fluid in stenosed arteries. Commun. Nonlinear Sci. Numer. Simul. **14**, 2971–2981 (2009)
Tzirtzilakis, E.E.: Biomagnetic fluid flow in a channel with stenosis. Physica D **237**, 66–81 (2008)
Yang, N., Vafai, K.: Modeling of low-density lipoprotein (LDL) transport in the artery effects of hypertension. Int. J. Heat Mass Transf. **49**, 850–867 (2006)
Yang, N., Vafai, K.: Low-density lipoprotein (LDL) transport in an artery—A simplified analytical solution. Int. J. Heat Mass Transf. **51**, 497–505 (2008)